Construction and Building Materials 342 (2022) 128067

Contents lists available at ScienceDirect

Construction and Building Materials

journal homepage: www.elsevier.com/locate/conbuildmat

Influence of the type and concentration of the activator on the microstructure of alkali activated SiMn slag pastes

R. Navarro [a], E. Zornoza [a,*], I. Sánchez [a], E.G. Alcocel [b]

[a] Dept. of Civil Engineering. University of Alicante, Spain
[b] Dept. of Architectonic Constructions. University of Alicante, Spain

ARTICLE INFO

Keywords:
SiMn slag
Alkali activation
Pastes
Microstructure

ABSTRACT

The influence of the type and concentration of the activator on the composition of the products formed and the microstructural development of alkali activated SiMn slag pastes and their evolution with curing time are studied. About 15–17 million tons of SiMn slag is produced per year, so valorising this residue is interesting for the economic and environmental scope. For this purpose, NaOH and WG with different concentrations of Na_2O have been used as activators. The hydration products have been studied by X-ray diffraction analysis (XRD) and thermogravimetric analysis (TGA). Scanning electron microscopy (SEM) combined with energy dispersive spectroscopy (EDX) has been used to study the microstructure and elemental composition of hydrated phases. The advance of the degree of hydration with time and with the activator concentration is consistent with the mechanical behaviour of these pastes observed in previous studies. All the pastes show high microcracking due to the stresses caused by the shrinkage, as it has been observed in previous studies. Elemental composition data do not show significant differences regarding the type of activator with respect to the main elements and their relationship in the reaction products except for Mn. The main reaction product formed in the alkaline activation of SiMn slag is C-S-H with a low Ca/Si ratio, this being higher for pastes activated with NaOH compared to those with WG. In addition, the modification of the C-S-H structure is demonstrated by the presence of small amounts of Al and Mn and that Mg is not incorporated into it. The presence of hydrotalcite is not detected by XRD, but small amounts have been confirmed by TGA/DTG and SEM/EDX.

1. Introduction

At present, both the different international laws and the demands of society require the development of a sustainable construction. Reducing the use of natural raw materials and CO_2 emissions are two necessary actions in the manufacture of construction materials and, more specifically, in the manufacture of binders with technical performance comparable to those of Portland cement. A widely explored alternative [1–3] is the recovery of industrial by-products as raw material for the manufacture of alkali activated binders, which have been developed from the bases proposed by Glukhovsky in 1957 [1]. However, the great variety of products studied makes it necessary to adjust the optimal conditions for an efficient development of the binder in each case.

The microstructure of the paste and the chemical structure of the cementitious products formed during the alkaline activation will strongly affect the final most interesting properties of these type of materials: mechanical resistance and durability [4]. Alkali activated binders are obtained through the reaction of a precursor (typically, in a general sense, an aluminosilicate) with an alkaline activator [4–6]. The chemical composition and initial conditions of the precursor will determine, in addition to the activation conditions, the chemical structure of the products formed, the microstructure of the paste and the final properties, consequently generating binders with specific properties. In general, they are classified into two large groups: low-calcium precursors, fundamentally consisting of alumina and silica, such as fly ash and residues of similar composition, or moderately calcium-rich precursors, such as blast furnace slag and residues of similar composition [1,4,7].

Previous works [8–11] have demonstrated that it is possible to valorise SiMn slag as a raw material (precursor) for the manufacture of alkali activated binders. This waste material comes from the manufacture of silico-manganese alloys, generating between 1.2 and 1.4 tons of waste for each ton of alloy produced [11], which represents between 15 and 17 million tons of waste per year. SiMn slag has a silico-calcic nature similar to blast furnace slag, but with a different chemical composition, mainly due to its lower calcium content and high manganese content

* Corresponding author.

https://doi.org/10.1016/j.conbuildmat.2022.128067
Received 16 March 2022; Received in revised form 17 May 2022; Accepted 4 June 2022
Available online 11 June 2022

(>10%). It has been shown that the SiMn slag can be activated with both sodium hydroxide (NaOH) and waterglass (WG) with good mechanical and durability results [8–10], without the need to subject the residue to prior activation processes that reduce the balance of the energy efficiency of its recovery process [3]. The only requirement is to reduce its particle size to values similar to those needed for regular binders. These properties, mechanical strength and durability, linked to the microstructural development of the pastes, depend on the structure and composition of the slag, the type and concentration of activator, and the curing conditions of the pastes [12–17].

Regarding the influence of the slag, many studies have been carried out with slags of different origin and composition. According to several authors [12,18–20], the main products formed after slag activation, regardless of the type of activator, are hydrated calcium silicates (C-S-H) and hydrotalcite. However, the structure and composition of C-S-H with the inclusion of Al or Na in the structure, the way in which hydrotalcite appears, the incorporation of Mn into the gel structure or the existence of other minor phases, has been shown to be clearly dependent on the raw material [11,16,21–23].

On the other hand, it has also been shown that the nature of the activator (type and concentration) has a strong influence on the kinetics of the activation process and the microstructure of the pastes, determining the structure and composition of the hydrated products formed as well as the their porous structure [15,17,21,24–26]. In any case, both compounds (C-S-H and hydrotalcite) are responsible for their mechanical resistance and durability. Specifically, hydrotalcite plays a very important role in several properties related to durability, such as carbonation [23], chloride binding [27] and sulphate resistance [28].

Many studies on binders based on alkali activated slags have been published in the last several decades. As a result, it has been clearly established the great influence that the raw material exerts on the optimal activation conditions, as well as the type and characteristics of the reaction products and the final properties. Previous studies using SiMn slag as precursor showed optimal activation conditions [8] and developed properties [9,10] demonstrating its feasibility of use.

The objective of this work is to deepen the knowledge about binders manufactured with SiMn slag. The influence of the type and concentration of the activator on the composition of the products formed and the microstructural development of alkali activated SiMn slag pastes and their evolution with curing time are studied. For this purpose, NaOH and WG with different concentrations of Na_2O have been used as activators. Pastes have been prepared with 3 different concentrations of each activator, which have been cured at 7, 28 and 90 days. For all the pastes, the hydration products have been studied by X-ray diffraction analysis (XRD) and thermogravimetric analysis (TGA). Scanning electron microscopy (SEM) combined with energy dispersive spectroscopy (EDX) has been used to study the microstructure and elemental composition of hydrated phases.

2. Experimental

2.1. Raw materials

A Spanish SiMn granulated slag supplied by Ferroatlántica plant placed at Boo-de-Guarnizo (Cantabria, Spain) was used. The chemical composition of the slag, obtained by X-ray fluorescence (XRF), is presented in Table 1.

(1) L.O.I.: Loss on ignition at 950 °C for 1 h.

In a previous work [8], it was concluded that the present slag can be classified as acid slag with moderate hydraulicity according to its basicity index (0.73) and its hydraulicity index (0.85) [29–31].

SiMn slag has a vitreous content of 96.0 ± 1.5%. The vitreous phase was determined by X-ray diffraction in a PANalytical diffractometer (EMPYREAN). The complete identification and quantification have been determined by Rietveld method [32] using quartz as standard sample, $MoK_{\alpha 1}$ radiation, a scan from 3° to 35°, for 5 h in 0.0113° steps, at 50 kV and 50 mA.

The determination of reactive silica (33.80%) and insoluble residue (3.35%) of the SiMn slag was made according to standards UNE 80225–2012 and UNE-EN 196–2-2014 [33,34]. According to the slag chemical composition, its relatively high content of reactive silica and its vitreous phase proportion, the alkali activation procedure should be successfully implemented on this material, which is also in accordance with previous studies [8,30,35].

SiMn original granulated slag was ground prior to its use in a laboratory ball mill (Nanneti model SPEEDY 1). After 25 min of grinding, the resulting slag has a fineness of 5512 cm^2/g. The specific surface of the material was found by applying the Blaine's air permeability method [36]. According to Wang et al. [31], this value is within the optimal fineness range for acid slags similar to that used in this research, 4500–6000 cm^2/g. Furthermore, a laser diffraction equipment (Malvern Instruments, model Mastersizer 2000) was used to determine the size and particle distribution of the slag. The particle size range of slag was 0.32–113.58 μm, with a $D_{V,50}$ = 9.2 μm and a $D_{4,3}$ = 15.2 μm. The density of this SiMn slag is 2.916 g/cm^3 [37].

Alkaline solutions used to activate the SiMn slag were prepared with a commercial sodium silicate (Na_2SiO_3 (neutral solution QP, Panreac): SiO_2/Na_2O molar ratio = 3.28) and sodium hydroxide (technical grade, Panreac). Two different types of activators and three different activator concentrations have been tested: NaOH solution with a 3.0%, 3.5% and 4.0% of Na_2O; and a waterglass solution (WG) with a 4.0%, 4.5% and 5.0% of Na_2O. NaOH activating solutions were prepared by solving the required amount of sodium hydroxide in distilled water. WG solutions were fabricated by mixing sodium silicate and sodium hydroxide in the appropriate quantities and the subsequent dilution of the mix with distilled water. The SiO_2/Na_2O ratio of the WG solution was set to 1.00. For the WG activator and the NaOH activator, a solution/slag ratio of 0.375 and 0.35 were used, respectively. These activating solutions were selected according to the particular findings of a previous research [8–10].

2.2. Preparation of pastes

All pastes were prepared by the mixing of 1800 g of ground granulated SiMn slag and the calculated quantity of alkaline solutions, in a mixer Controls Automix (model 65-L0006/A) according to the standard UNE EN 196–3 [38]. All specimens have been cured in a humid chamber with a 100% of relative humidity (RH) and 20 ± 2 °C for 7, 28 and 90 days.

2.3. Analysis techniques

2.3.1. X-ray diffraction

X-ray diffraction (XRD) data were collected using a Bruker D8-Advance with mirror Göebel (non-planar samples), with a generator of X-ray KRISTALLOFLEX K 760-80F (power: 3000 W, voltage: 20–60 kV and current: 5–80 mA), fitted with a tube of X-ray with copper anode. The samples were scanned using incident beam monochromator with

Table 1
Chemical composition of the SiMn slag determined by X-ray fluorescence analysis.

Component	SiO_2	CaO	MnO	Al_2O_3	MgO	Fe_2O_3	K_2O	Na_2O	SO_3	Cl	BaO	P_2O_5	SrO	TiO_2	ZrO_2	L.O.I.(1)
Mass % as oxide	36.53	29.10	12.23	9.86	4.69	0.92	1.08	0.34	2.77	0.16	1.60	0.35	0.14	0.19	0.04	−1.25

CuKα radiation (λ = 1.54 Å) at room temperature between 2.5° and 70° 2θ with a step increment of 0.05°, at an angular velocity of 1°min^{-1}, at 40 kV and 40 mA.

2.3.2. Thermogravimetric analysis

TGA was performed between 25 and 1100 °C at a heating rate of 10 °C/min in N_2 atmosphere (100 ml/min) in a Mettler Toledo TGA/DSC2.

2.3.3. Scanning electronic microscopy

Scanning electron microscope Hitachi S3000N (SEM) equipped with an energy dispersive X-ray detector Bruker XFlash 3001 (EDX) was used for microanalysis and mapping of pastes. With the help of this technique, it was possible to carry out the elemental analysis of the content of each element in order to study the relationships between different elements in the formation of pastes. Slices of hydrated samples were cut, immediately immersed in acetone and subsequently dried at 40 °C for 24 h for the microscopical investigations. They were then impregnated using a low viscosity epoxy resin and polished down to a thickness between 30 and 40 μm. Finally, the surface is covered with a layer of carbon.

3. Results and discussion

3.1. Evolution of microstructure based on XRD analysis

An analysis of the literature shows that the phases formed depend on the type and concentration of activator, the structure and composition of the slag and the curing conditions of the pastes. Normally in granulated blast furnace slag (GBFS), the main reaction product is the C-A-S-H gel (if the Ca/Si ratio is lower than 1–1.3), in addition to a series of secondary products that include hydrotalcite, calcite and aluminate ferrite monosulfate (AFm) type phases [1,18,39].

Figs. 1 and 2 show the identified phases in mineralogical analysis carried out through XRD on the pastes at 7, 28 and 90 days for the NaOH and WG activators, respectively.

For both activators the same phases are detected: Quartz (PDF 33–1161) (Q), Calcite (PDF 05–0586) (C), Alabandite (MnS) (PDF 01–1089) (A) and Calcium Aluminum Silicate ($Ca_2Al_2SiO_7$) (PDF 34–1236) (S). The presence of Alabandite in the pastes, the remaining phase of the unreacted slag, is expected since the quantification of the slag phases carried out by XRD in previous works [8] detects 2 ± 1% of this crystallized phase together with a 2 ± 1% graphite and 96 ± 1.5% vitreous phase. For pastes activated with NaOH, the presence of Akermanite ($Ca_2Mg(Si_2O_7)$) (PDF 76–0841) seems doubtful in those cured at 7 days, and its presence cannot be confirmed at 28 and 90 days. For those activated with WG, Akermanite was not detected at any curing age, which confirms that, in general, the pastes activated with WG present more disordered structures.

For both activators, when the curing time increases, it is observed that the background noise increases in the XRD spectra, which reports the increase in the amorphous phase in the structure, that is, the sample becomes less crystalline, making it practically impossible to detect the hydrated calcium silicates. The intensity of the crystalline peaks gradually decreases due to the formation of amorphous and/or poorly crystallized calcium silicate gel phases. The results obtained do not allow the presence of C-S-H (PDF 033–0306) and C-S-H (I) (PDF 034–0002) to be detected with certainty, as it has been established by other authors for slag pastes of similar composition [11,21,40,41] through peaks at 7°, 29° and 49.5° of 2θ. In the studied samples, for both activators and all concentrations and curing ages, no peaks are detected at 7° of 2θ, the peak at 29° is overlapped with Calcite whose presence is observed by TGA and DTA, and at 49.5° of 2θ overlaps with C-A-S (PDF 34–1236) and with MnS (PDF 01–1089). The C-S-H peak detected in a very overlapping way in this case at 29° of 2θ, it is not easy to attribute it to a specific composition with a given Ca/Si ratio, since it is detected by other authors with Ca/Si ratios from 0.8 to 1.7 [42]. In the studied

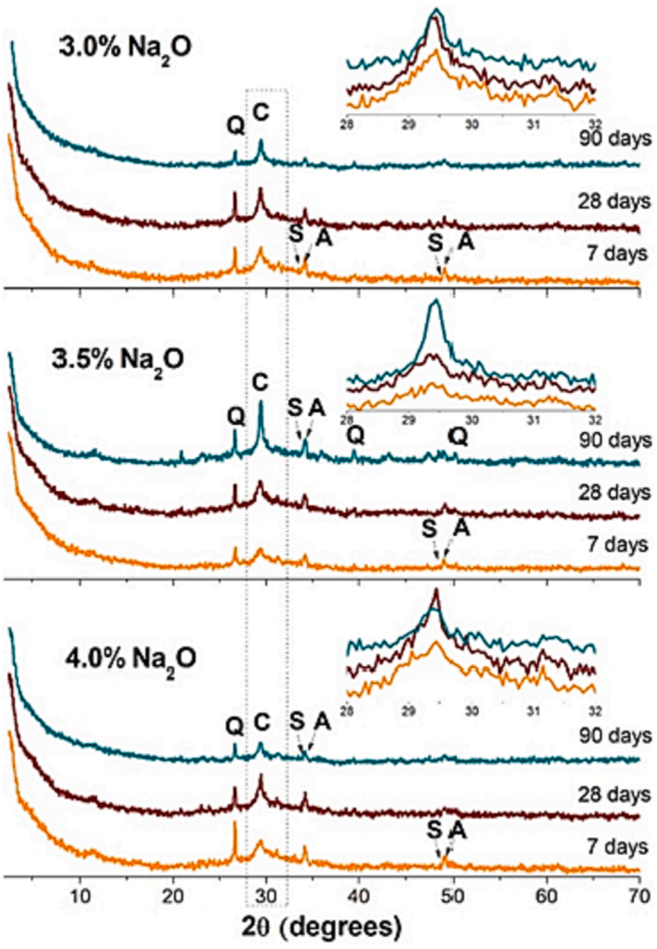

Fig. 1. XRD of pastes prepared with NaOH at three different concentrations (3.0, 3.5 and 4.0% Na_2O) and cured for 7, 28 and 90 days. Q, C, S and A stand for quartz, calcite, calcium aluminium silicate and alabandite, respectively.

pastes, this ratio is between 1.21 and 1.79, as will be shown later in Table 3. The existence of poorly crystalline C-S-H phases in granulated blast furnace slag pastes has been recorded by other authors, showing that those activated with NaOH lead to more crystalline phases than those activated with WG [12,22,25,41]. The possible difference could be due to the fact that these authors use concentrations of alkalis and SiO_2/Na_2O ratio much higher than those used in this study. Hydrotalcite ($Mg_6Al_2CO_3(OH)_{16}4H_2O$) (PDF 01–089-0460 or PDF 00–014-0191) has not been detected in any of the pastes studied; however, its presence has been confirmed by TGA, DTG and SEM/EDX as will be seen later. These results are in agreement with the moderate concentration of Mg in the slag (4.6%) that supposes a Mg/Al ratio of approximately 0.5, very far from the Mg/Al ratio of 3 that natural hydrotalcite presents [12].

The presence of AFm-type secondary phases (Stratlingite (C_2ASH_8) (PDF 00–029-0285)) was detected in slag pastes activated with NaOH [12], although in other later studies it has not been detected [21,25,41]. Other authors relate its detection to higher alumina contents in the slag [16]. Previous studies detected Stratlingite (C_2ASH_8) in mechanically activated SiMn slag pastes prior to alkaline activation with NaOH [11]. However, it has not been possible to detect its presence in any of the SiMn pastes studied, due to the moderate Al_2O_3 content of this slag (9.86%) and the larger particle size than that used in the present work.

On the other hand, in none of the pastes crystalline phases containing alkaline cations have been detected by XRD, a result that coincides with other authors [11,12,21,41].

Finally, the absence of crystalline phases containing Mn suggests that manganese is incorporated together with Mg into the amorphous phases.

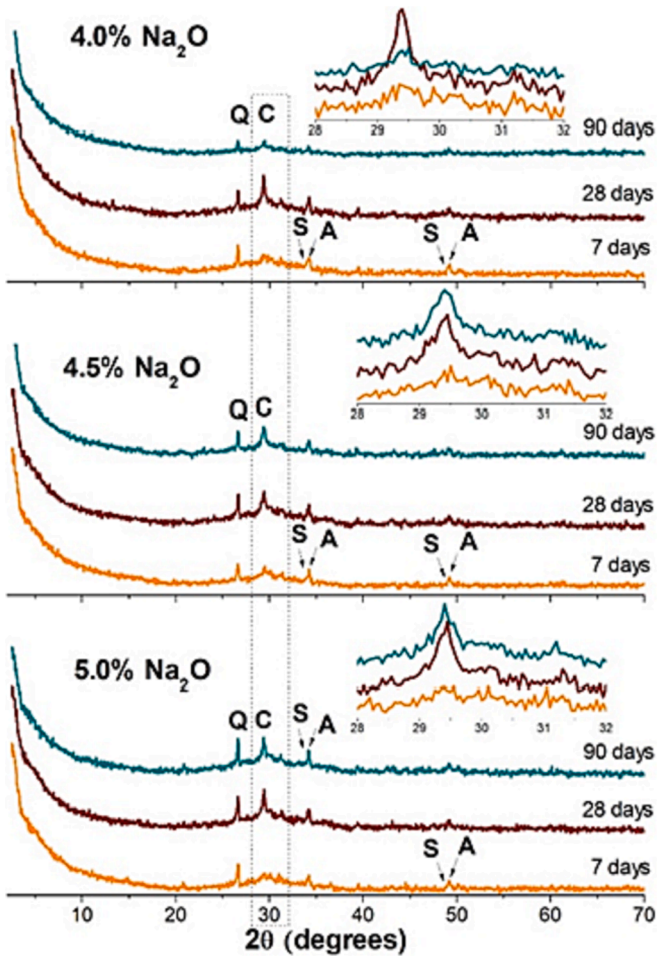

Fig. 2. XRD of pastes prepared with WG at three different concentrations (4.0, 4.5 and 5.0% Na_2O) and cured for 7, 28 and 90 days. Q, C, S and A stand for quartz, calcite, calcium aluminium silicate and alabandite, respectively.

However, after the activation of SiMn slag very similar to the one used in this study with NaOH, other authors [11] detected C-S-H phases with low degree of crystallinity (PDF 09–0210 and PDF 33–0306); calcium carbonate; hydrotalcite and calcium magnesium aluminate hydrate ($(C,M)_4AH_{13}$) at 28 days by XRD, the latter overlapping with hydrotalcite. Other works also carried out with SiMn slag detected the presence of crystalline compounds that incorporate manganese such as MnO and $MnSiO_3$. These compounds are considered as remaining phases of the unreacted slag since its analysis before activation offered the same species [43]. In both cases, the differences in the origin of the slag, in the granulation treatment together with the different specific surface obtained after the grinding process and/or mechanical activation could be the causes of these differences with respect to the results obtained in this study.

3.2. Evolution of microstructure based on TGA/DTG analysis

Figs. 3 and 4 show the results of TGA (weight loss %) and DTG (mg/s) performed in the pastes studied for each of the activators, NaOH and WG, respectively. In them, it can be clearly observed, regardless of the type and concentration of the activator, the evolution over time of the microstructure of the pastes, since the differential curves made at 7 and 28 days are similar in all cases and at the same time markedly different of those obtained at 90 days, where a greater amount of reaction products is observed. These results are consistent with the mechanical results obtained in previous studies [8,9].

Figs. 3 and 4 show, for both activators, at all concentrations and at all

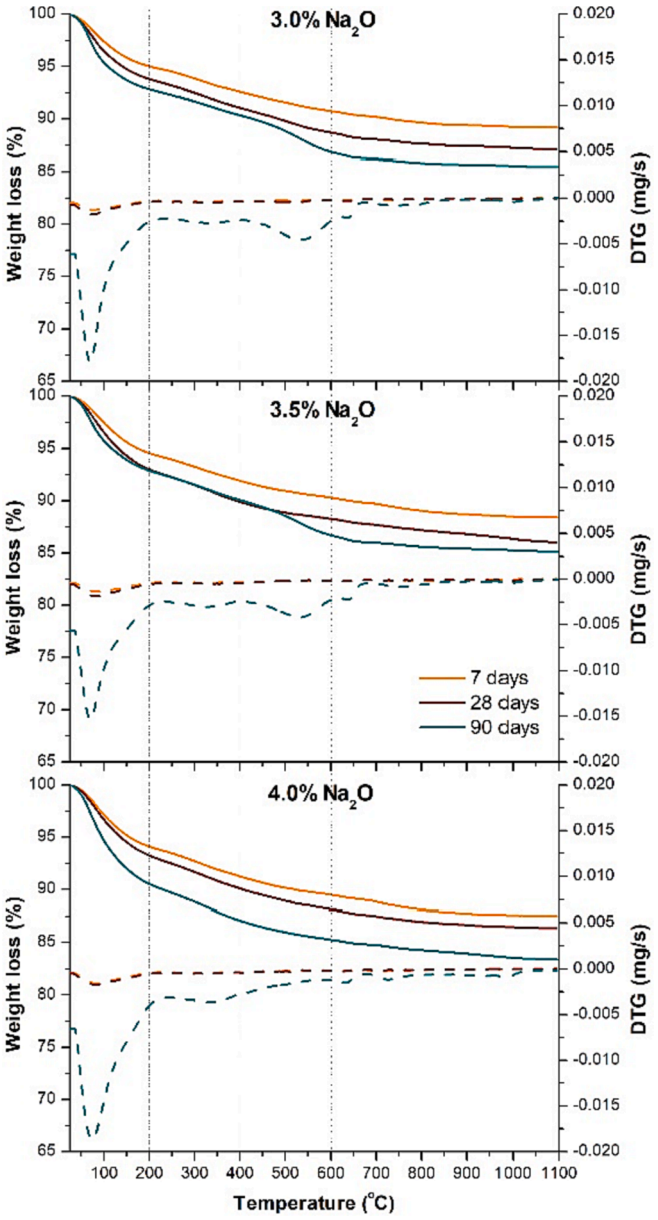

Fig. 3. TGA and DTG of pastes prepared with NaOH at three different concentrations (3.0, 3.5 and 4.0% Na_2O) and cured for 7, 28 and 90 days.

curing ages, a main band between 50 and 200 °C, which can be attributed to the water present in the reaction products formed during the activation reactions. Therefore, these weight losses between 50 and 200 °C are indicative of C-S-H dehydration, as it has been established by other authors for slags of similar composition [12,16,40,41]. In this way, the presence of C-S-H is confirmed and it is shown that it is the main reaction product formed in the alkaline activation of SiMn slag regardless of the type and concentration of the activator used, despite not having been clearly identified by XRD due to overlapping with the carbonates and its mainly amorphous structure.

Focusing only on the results at 90 days, the samples activated with NaOH show the presence of hydrotalcite phase, which could not be detected by XRD. Hydrotalcite exhibits a brucite-like layer-based structure ($Mg(OH)_2$) with water molecules and anions CO_3^{2-} between the layers, although many other anions can occupy interlayer positions in the phases that form in activated slag pastes [12]. Losses between 200 and 400 °C, with a maximum around ~ 330 °C, are attributed to its decomposition [12,16,40,41], mainly due to the dehydroxylation of the

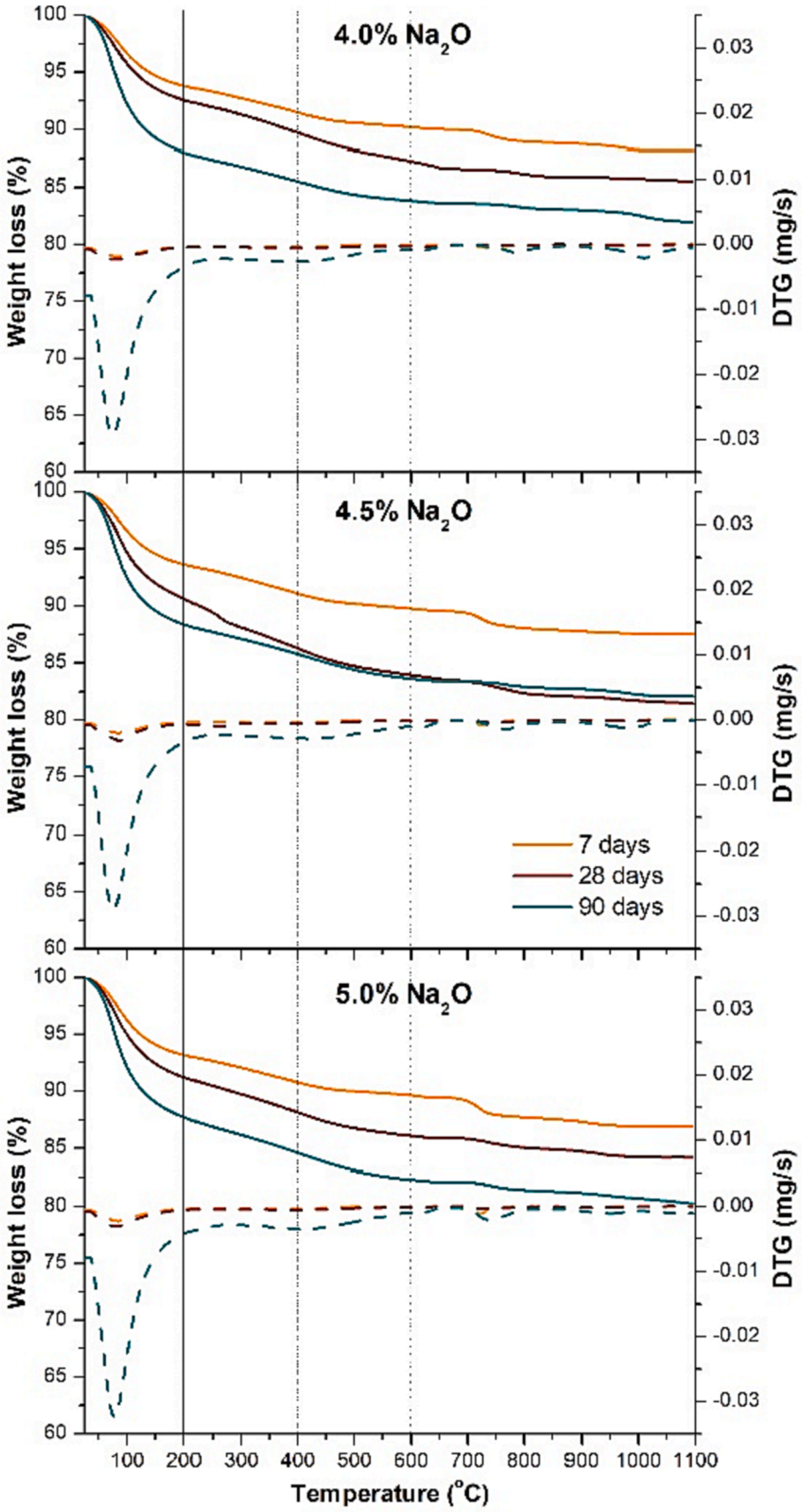

Fig. 4. TGA and DTG of pastes prepared with WG at three different concentrations (4.0, 4.5 and 5.0% Na_2O) and cured for 7, 28 and 90 days.

brucite layers that are present in the hydrotalcite structure [44]. In addition, the loss between 400 and 600 °C (~535 °C), detected for the lowest concentrations of activator, is fundamentally due to the progressive elimination of hydroxyl ions, generating the metallic oxide and the spinel structure ($MgAl_2O_4$) [44]. Finally, the loss between 600 and 700 °C (~635 °C) is attributed both to the hydrotalcite-type phase and to those produced by other carbonates detected by XRD [40,44]. In any case, the differences in weight losses indicate that much less hydrotalcite than C-S-H has been formed, in a qualitative way, a result that is consistent with the relatively low presence of MgO in the SiMn slag. The formation of small amounts of hydrotalcite is confirmed by the elemental composition study carried out by SEM/EDX as it will be shown later. Finally, the losses detected above 700 °C are attributable to the decomposition of other carbonates present in the samples, fundamentally due to exposure to the air of the samples (losses between 600 and 700 °C, 700–850 °C and 850–1050 °C). The identification of hydrotalcite occurs more clearly for the two lowest activator concentrations.

In pastes activated with WG and cured at 90 days, a very wide band of loss is observed between 200 and 650 °C with a very wide maximum above 420 °C, which could also be attributed to the presence of hydrotalcite [40]. In addition, losses attributable to carbonates are detected, between 650 and 850 °C attributable mainly to calcite; and between 900 and 1050 °C to other carbonates with a more perfect crystalline structure.

Comparing the results between both activators, a greater formation of hydrotalcite (higher intensity peak) is detected in pastes activated with NaOH than in those with WG, which is consistent with what was observed by other authors for slag pastes of similar composition [41]. This fact contributes to enhance the CO_2 absorption and improving the resistance to carbonation of pastes activated with NaOH [23]. However, according to Shi et al [41], the results of previous studies with SiMn slag do not agree with this statement [10]. In addition to the amount formed, variations in the maximum temperatures are also detected, which suggests, according to other authors [45], variations in the composition and/or structure of the hydrotalcite depending on the type and concentration of the activator.

The content of bound water in the structure of the formed phases has been used as a measure of the degree of hydration of the activated slag [20,21,40]. Table 2 shows the bound water content calculated from the TGA data and expressed as total weight loss of the pastes between 25 and 650 °C.

These values show the progress of the degree of hydration with time and with the concentration of activator regardless of the activator. These results are consistent with the mechanical behaviour of these pastes observed in previous studies [8] and with those that have shown that there is an adequate correlation between the content of bound water in the structure and the compressive strength of the pastes [40]. Regarding the type of activator, pastes activated with NaOH show lower weight losses, therefore, a lower degree of hydration than pastes activated with WG. At 7 days, they reach a similar degree of hydration regardless of the activator used. However, after 28 days the differences are clearly evident. This difference between the activators and the magnitude of the bound water values in the reaction products are similar to those found by other authors with GBFS [20,21]. In any case, these results alone do not allow to conclude on the degree of reaction of the slag as a function of the activator, since it has been previously established that the reaction products formed using WG incorporate much more water than those formed when NaOH is used as activator, an aspect that makes it difficult to compare them [16,20].

Table 2
Weight loss from TGA (25–650 °C) in wt % of the alkali activated slags.

	NaOH			WG		
Age (days)	3.0% Na_2O	3.5% Na_2O	4.0% Na_2O	4.0% Na_2O	4.5% Na_2O	5.0% Na_2O
7	9.63	10.07	10.85	9.97	10.42	10.57
28	11.77	12.10	12.27	13.27	16.42	14.14
90	13.67	13.87	15.09	16.39	16.61	17.90

3.3. Evolution of microstructure based on EDX analysis

Energy dispersive X-ray analysis (EDX) has been used to determine the elemental composition of the phases of the microstructure in order to compare the influence of the type and concentration of activator on the chemical composition of the products formed. Fig. 5 shows the SEM images of pastes activated with NaOH (4.0% Na_2O) and WG (4.5% Na_2O) cured for 7, 28 and 90 days, which are representative of the microstructure of the pastes studied since no significant differences have been observed between them. The images reveal the progressive formation of products and the development of the microstructure, clearly evidencing two zones in it: unreacted slag particles and a matrix formed by the reaction products. Some unreacted slag particles are shown in Fig. 5 as an example. The presence of unreacted particles is still evident after 90 days of curing. As can be seen in the images, a dense matrix is observed between slag particles and it has not been possible to clearly detect the presence of rings of reaction products around the unreacted slag particles, as other authors have detected [14,16,17,21,25]. The absence of such rings suggests that the formation of products occurs from nucleation from dissolution for all the studied pastes, regardless of the type of activator [17]. All the pastes, regardless of the activator and its concentration, show high microcracking due to the stresses caused by the shrinkage experienced by this material, as it has been observed in previous studies [8,9]. The cracks run through both the matrix of reaction products and the faces of the unreacted slag particles.

Microanalyses of the hydration products in the SEM were also performed at different curing ages. It was not possible to obtain distinct analyses from regions of different phases, indicating that the products were intermixed on the scale of the microanalysis probe (interaction volume ~ 1 μm^3) [14]. Table 3 shows the main elements and their relationship in the reaction products obtained for the matrix of all the pastes studied. The values given in Table 3 represent the mean of at least 25 individual EDX analyses. An outliers elimination study has been carried out on the individual results [46] and subsequently the mean value and the confidence interval have been calculated. In addition to the amounts of Ca and Si, significant amounts of Mg, Al and Mn have been detected in all the samples. The presence of Na has not been detected, as other authors have found [12,25], probably because free Na has been eliminated in the sample preparation process. From the elemental composition data, no significant differences can be established with respect to the type of activator, except for the higher Si content of the pastes activated with WG, as expected due to their composition. Regarding the curing time, Mg and Al practically remain the same and Ca, generally, increases with time.

On the other hand, for Mn, differences are detected depending on the activator. Observing the data between 7 and 90 days, in the pastes activated with NaOH it can be seen that the Mn increases with time but it decreases in the WG pastes, a result that is consistent with the greater dissolution capacity of the slag with NaOH compared to WG [20]. Regarding the concentration of the activator, in general, the higher the concentration, the higher the Ca and Mn content. However, Mg and Al present maximum values for 3.5% NaOH and 4.5% WG concentrations that coincide with those that offer the best mechanical behaviour [8,9] and that is consistent with that indicated by other authors about the influence of hydrotalcite-type phases in mechanical strength [22].

Table 3 also shows the Ca/Si and Mn/Ca ratios, both obtained from the average values for each of the pastes studied, but Mg/Al ratios (which can be related to presence of hydrotalcite) and Al/Ca ratio (which can show the introduction of Al in the C-S-H) are calculated according to the procedures established by Wang and Scrivener [12]. Regarding the Ca/Si ratio, it is observed that it is very similar to that of

Table 3
Elemental composition and atomic ratios in the hydrate phases obtained by EDX analyses (arithmetic average (%) ± confidence interval). The Mg/Al ratio was calculated accoding to [12].

(% ± C.I.)	Mg	Al	Si	Ca	Mn	Ca/Si	Mn/Ca	Mg/Al	Al/Ca
Slag	2.01 ± 0.11	3.54 ± 0.19	10.11 ± 0.51	15.99 ± 0.84	6.45 ± 0.35				
3.0%NaOH 7d	1.69 ± 0.43	3.02 ± 0.42	9.41 ± 1.18	12.99 ± 1.14	4.06 ± 0.37	1.38	0.31	0.97	0.09
3.0%NaOH 28d	1.40 ± 0.32	3.13 ± 0.21	9.22 ± 0.51	15.19 ± 0.86	4.51 ± 0.39	1.65	0.30	0.75	0.08
3.0%NaOH 90d	1.65 ± 0.20	3.11 ± 0.18	8.83 ± 0.56	13.72 ± 0.82	4.86 ± 0.44	1.55	0.35	0.83	0.08
3.5%NaOH 7d	1.87 ± 0.42	3.19 ± 0.34	9.07 ± 0.85	10.95 ± 0.75	3.82 ± 0.38	1.21	0.35	0.93	0.10
3.5%NaOH 28d	2.21 ± 0.17	3.63 ± 0.22	10.19 ± 0.57	14.62 ± 0.77	6.09 ± 0.54	1.43	0.42	0.72	0.03
3.5%NaOH 90d	2.05 ± 0.11	3.47 ± 0.16	9.54 ± 0.39	15.50 ± 0.76	5.20 ± 0.34	1.63	0.34	0.51	–
4.0%NaOH 7d	1.95 ± 0.19	3.40 ± 0.16	9.39 ± 0.31	14.54 ± 0.55	5.21 ± 0.30	1.55	0.36	0.85	0.08
4.0%NaOH 28d	1.48 ± 0.21	3.10 ± 0.19	8.58 ± 0.52	14.98 ± 0.87	4.24 ± 0.30	1.75	0.28	0.72	0.07
4.0%NaOH 90d	1.90 ± 0.27	3.27 ± 0.25	9.45 ± 0.55	15.67 ± 1.02	5.55 ± 0.49	1.66	0.35	0.82	0.07
4.0%WG 7d	2.20 ± 0.19	3.23 ± 0.44	9.71 ± 1.08	15.19 ± 1.30	4.72 ± 0.67	1.56	0.31	0.57	–
4.0%WG 28d	1.50 ± 0.14	2.83 ± 0.12	9.29 ± 0.47	16.68 ± 0.74	4.21 ± 0.21	1.79	0.25	0.79	0.05
4.0%WG 90d	0.58 ± 0.39	2.11 ± 0.20	7.12 ± 0.64	11.21 ± 0.77	3.23 ± 0.42	1.57	0.29	0.63	0.13
4.5%WG 7d	1.62 ± 0.16	3.01 ± 0.11	10.85 ± 0.50	14.44 ± 0.59	4.94 ± 0.23	1.33	0.34	1.01	0.10
4.5%WG 28d	0.96 ± 0.25	2.53 ± 0.15	8.64 ± 0.41	14.67 ± 0.71	4.05 ± 0.25	1.70	0.28	0.59	0.07
4.5%WG 90d	1.62 ± 0.15	3.00 ± 0.15	11.21 ± 0.61	14.86 ± 0.89	4.99 ± 0.28	1.33	0.34	0.78	0.06
5.0%WG 7d	1.92 ± 0.12	3.16 ± 0.16	11.25 ± 0.64	14.08 ± 0.91	5.29 ± 0.14	1.25	0.38	0.42	–
5.0%WG 28d	1.78 ± 0.18	3.02 ± 0.16	10.16 ± 0.48	14.19 ± 0.96	5.00 ± 0.41	1.40	0.35	0.82	0.06
5.0%WG 90d	1.38 ± 0.21	3.00 ± 0.20	10.97 ± 0.76	16.26 ± 0.79	4.82 ± 0.29	1.48	0.30	0.77	0.08

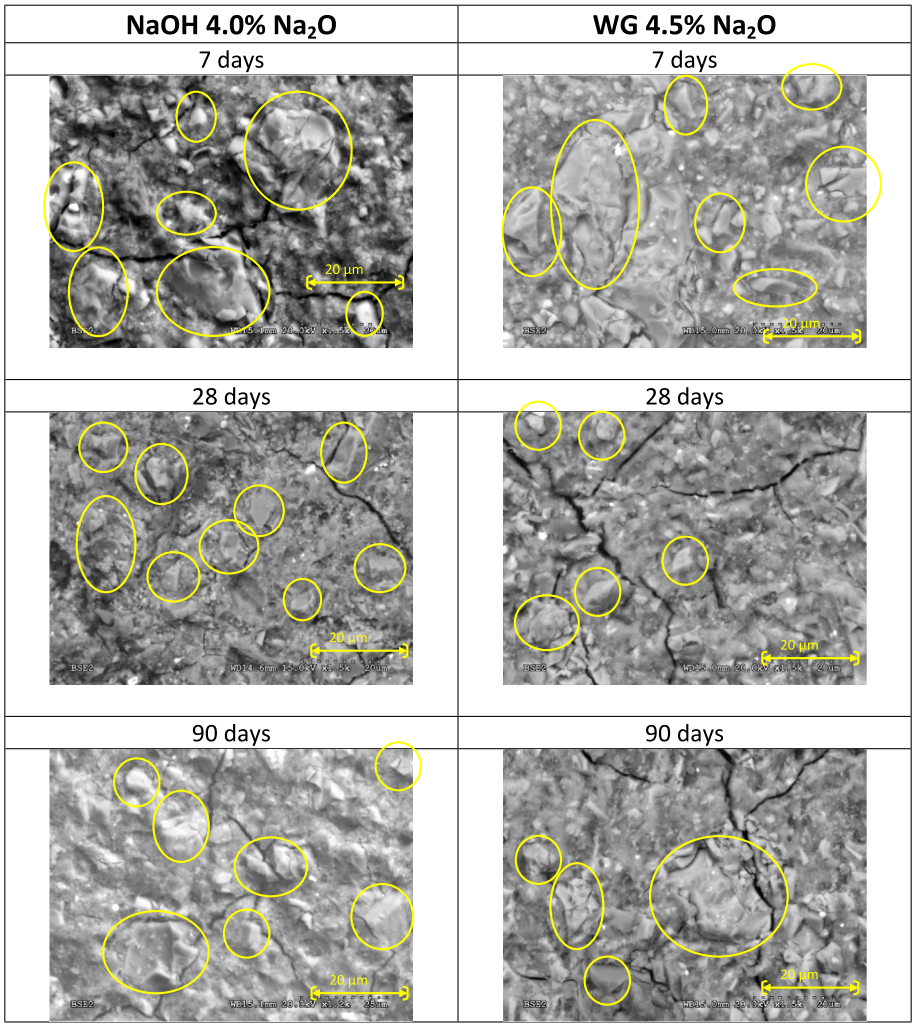

Fig. 5. SEM/EDX of pastes activated with NaOH (4.0% Na_2O) and WG (4.5% Na_2O) cured at 7, 28 and 90 days. Unreacted slag particles are circled. The magnification of all images is x1,500.

the unactivated slag and is not clearly influenced by the curing time. This result agrees with other authors [16]. The data show that regardless of the type of activator used, the main reaction product has been C-S-H with a low Ca/Si ratio, a result in agreement with [12] that have studied slags of similar composition. However, the nature of the activator influences the structure and composition of the hydrated calcium silicate

formed as a consequence of the alkaline activation of the slag [25]. It is observed in Table 3 that the pastes activated with NaOH generally present higher Ca/Si values and these ratios increase with the concentration of NaOH. On the contrary, the pastes activated with WG present a clear decrease in the Ca/Si ratio as the concentration of the activator increases due to a greater availability of the silicate species, in agreement with what has been established by other authors [17,20,25].

On the other hand, the data show that Mn is moderately incorporated into the paste structure since in all cases (for the two activators and for all curing ages) the Mn/Ca ratio (obtained directly from the analysis) is lower than that of the unreacted slag. In addition, regarding the distribution of Mn in the structure, the data show a high dispersion of this element in the sample. Using different relationships, it has not been possible to obtain an adequate linear relationship in most of the pastes that allows calculating the Mn/Ca or Mn/Si relationship to demonstrate the modification of C-S-H by the presence of Mn. For pastes cured at 90 days and activated with 4.5 and 5.0% WG, the representation of Mg/Ca versus Mn/Ca has allowed calculating Mn/Ca ratios of 0.04 and 0.1 when Mg/Ca tends to zero, respectively, which would demonstrate the entry of small amounts of Mn into the C-S-H, as it has been shown in previous studies by other authors [11]. The procedure for obtaining these values is calculated according to Wang and Scrivener [12]: for a particular sample, the linear fitting of Mg/Ca vs Mn/Ca is made (the values are obtained by the random sampling in the reacted paste by EDX); then, the presented value is the Mn/Ca value when Mg/Ca is zero in that linear fitting equation.

Fig. 6 shows the Mg/Ca versus Al/Ca ratio for pastes activated with NaOH (4.0% Na_2O) and with WG (4.5% Na_2O), at 90 days. With them, in both cases the formation of a minor phase rich in Mg and Al (hydrotalcite) is demonstrated, with values for the slope of 0.82 and 0.78 for NaOH and WG, respectively. This phase was detected by TGA but not by XRD. The value of the Mg/Al ratio calculated for all the pastes studied is also presented in Table 3, showing the formation of hydrotalcite in all the pastes, regardless of the type of activator, the concentration and the curing time. Since the values obtained are quite similar to each other, the type of hydrotalcite phase formed can be considered independent of the type of activator [20]. It has been described that the Mg/Al ratio is approximately 2 for the hydrotalcite phase of alkali activated slags with Mg/Al ratios for the unreacted slag between 0.8 and 1.5 [12,14,21,22]. The Mg/Al ratio of the slag used in this study is lower, which justifies the lower Mg/Al values for hydrotalcite observed in these pastes. Some authors [25] have detected shades of different intensity in the matrix, attributing the darkest to the presence of areas rich in Mg and the lightest to the presence of C-S-H. However, other authors [12] conclude that hydrotalcite-type phases cannot be distinguished in SEM images, as it has occurred in this study where the microstructural analysis carried out by BSE image shows the matrix without significant differences in colour (Fig. 5).

On the other hand, in Fig. 6, extrapolating the linear fitting to the Mg/Ca value = 0, the Al/Ca value has been obtained, which could only be assigned to C-S-H. These values are 0.07 for the pastes activated with NaOH and 0.06 for WG pastes. These results demonstrate the incorporation of Al in a small proportion in the C-S-H structure and also that Mg is not incorporated into the C-S-H structure [20,47]. Values calculated in the same way are shown for the rest of the pastes in Table 3, thus confirming the presence in all cases of small amounts of Al in the C-S-H structure, slightly higher for pastes activated with NaOH, as it has been previously described [25], and without significant dependence on the concentration of the activator [17].

In summary, the SEM data confirm that the main product has been in all the samples C-S-H, in whose structure a small amount of Al and Mn has entered. In addition, dispersed hydrotalcite has been formed in the matrix, but due to the fact that Mg is a minor element in the slag, it has not been possible to detect it by XRD and the amount detected by TGA has been very low in relation to the C-S-H gel.

4. Conclusions

XRD, TGA and SEM have been used to characterize the main reaction products formed in alkali activated SiMn slag pastes with NaOH and WG, at different concentrations, and as a function of the curing time. The following conclusions have been obtained:

1. Regardless of the activator, the advance of the degree of hydration with time and with the activator concentration is consistent with the mechanical behaviour of these pastes observed in previous studies.

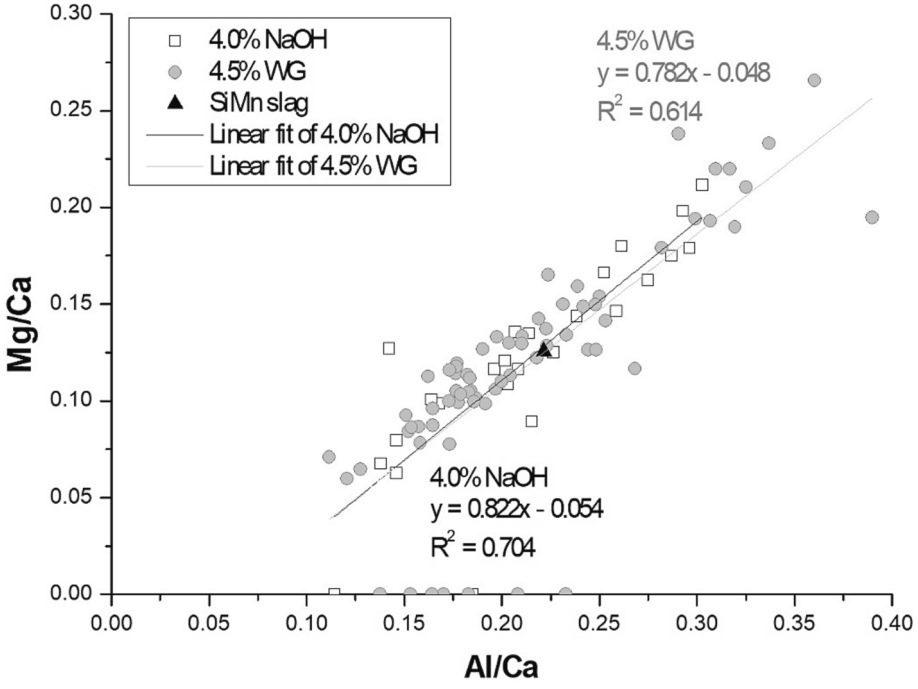

Fig. 6. Mg/Ca vs Al/Ca ratio plot for analyses of SiMn slag activated with NaOH (4.0% Na_2O) and WG (4.5% Na_2O) cured at 90 days.

All the pastes show high microcracking due to the stresses caused by the shrinkage experienced by this material, as it has been observed in previous studies.

2. Elemental composition data do not show significant differences regarding the type of activator with respect to the main elements and their relationship in the reaction products except for Mn. Mn increases with time in pastes activated with NaOH, a result consistent with the greater dissolution capacity of NaOH compared to WG.
3. It is shown that the main reaction product formed in the alkaline activation of SiMn slag, regardless of the type and concentration of the activator used, is C-S-H with a low Ca/Si ratio, this being higher for pastes activated with NaOH compared to those with WG. In addition, the modification of the C-S-H structure is demonstrated by the presence of small amounts of Al and Mn and that Mg is not incorporated into it.
4. Regardless of the type of activator, its concentration and curing time, and due to the moderate concentration of Mg in the slag, the presence of hydrotalcite is not detected by XRD. The existence of small amounts of hydrotalcite is confirmed by TGA/DTG; being its presence greater in pastes activated with NaOH than in those of WG. By SEM/EDX the formation of hydrotalcite is also confirmed for all pastes.

These results allow us to conclude that the alkaline activation of the SiMn slag presents a composition of hydrated products and a microstructure similar to that obtained with other slags widely studied for the manufacture of alternative alkaline activated binders to Portland cement. Therefore, the viability of valorizing the SiMn residue for this application is demonstrated.

Declaration of Competing Interest

The authors declare that they have no known competing financial interests or personal relationships that could have appeared to influence the work reported in this paper.

Acknowledgements

The authors wish to thank the Spanish Ministry of Science and Innovation for project funding (PID2020-118322RB-I00) through the *"Programa Estatal de I + D + i Orientada a los Retos de la Sociedad"* included in the *"Plan Estatal de Investigación Científica y Técnica y de Innovación 2017-2020"*. The authors also wish to thank Cristina Rodríguez from Ferroglobe, for the supply of SiMn slag necessary to carry out this research.

References

[1] A. Palomo, P. Krivenko, I. Garcia-Lodeiro, E. Kavalerova, O. Maltseva, A. Fernández-Jiménez, A review on alkaline activation: new analytical perspectives, Mater Construcción 64 (315) (2014) e022, https://doi.org/10.3989/mc.2014.v64.i31510.3989/mc.2014.00314.

[2] J.L. Provis, J.S.J. van Deventer, Alkali Activated Materials: State-of-the-Art Report, RILEM TC 224-AAM, Springer 13 (2014) 388.

[3] J.L. Provis, A. Palomo, C. Shi, Advances in understanding alkali-activated materials, Cem Concr Res 78 (2015) 110–125, https://doi.org/10.1016/j.cemconres.2015.04.013.

[4] J.L. Provis, Geopolymers and other alkali activated materials: Why, how, and what? Mater Struct Constr 47 (1-2) (2014) 11–25, https://doi.org/10.1617/s11527-013-0211-5.

[5] C. Shi, A. Fernandez Jimenez, A. Palomo, A.F. Jiménez, A. Palomo, New cements for the 21st century: The pursuit of an alternative to Portland cement, Cem Concr Res 41 (2011) 750–763, https://doi.org/10.1016/j.cemconres.2011.03.016.

[6] M.C.G. Juenger, F. Winnefeld, J.L. Provis, J.H. Ideker, Advances in alternative cementitious binders, Cem Concr Res 41 (12) (2011) 1232–1243, https://doi.org/10.1016/j.cemconres.2010.11.012.

[7] S.A. Bernal, J.L. Provis, D.J. Green, Durability of alkali-activated materials: Progress and perspectives, J Am Ceram Soc 97 (4) (2014) 997–1008, https://doi.org/10.1111/jace:12831.

[8] R. Navarro, E. Zornoza, P. Garcés, I. Sánchez, E.G. Alcocel, Optimization of the alkali activation conditions of ground granulated SiMn slag, Constr Build Mater 150 (2017) 781–791, https://doi.org/10.1016/j.conbuildmat.2017.06.064.

[9] R. Navarro, E.G. Alcocel, I. Sánchez, P. Garcés, E. Zornoza, Mechanical properties of alkali activated ground SiMn slag mortars with different types of aggregates, Constr Build Mater 186 (2018) 79–89, https://doi.org/10.1016/j.conbuildmat.2018.07.093.

[10] Navarro R, Alcocel EG, Sánchez I, Garcés P, Zornoza E. Corrosion resistance of steel reinforcements embedded in alkali activated ground granulated SiMn slag mortars. Constr Build Mater 2020;230. doi:10.1016/j.conbuildmat.2019.116917.

[11] S. Kumar, P. García-Triñanes, A. Teixeira-Pinto, M. Bao, Development of alkali activated cement from mechanically activated silico-manganese (SiMn) slag, Cem Concr Compos 40 (2013) 7–13, https://doi.org/10.1016/j.cemconcomp.2013.03.026.

[12] S.-D. Wang, K.L. Scrivener, Hydration products of alkali activated slag cement, Cem Concr Res 25 (3) (1995) 561–571, https://doi.org/10.1016/0008-8846(95)00045-E.

[13] T. Bakharev, J.G. Sanjayan, Y.-B. Cheng, Alkali activation of Australian slag cements, Cem Concr Res 29 (1) (1999) 113–120, https://doi.org/10.1016/S0008-8846(98)00170-7.

[14] A.R. Brough, A. Atkinson, Sodium silicate-based, alkali-activated slag mortars - Part I. Strength, hydration and microstructure, Cem Concr Res 32 (6) (2002) 865–879, https://doi.org/10.1016/S0008-8846(02)00717-2.

[15] Fernández-Jiménez A, Puertas F, Sobrados I, Sanz J. Structure of calcium silicate hydrates formed in alkaline-activated slag: Influence of the type of alkaline activator. J Am Ceram Soc 2003;86:1389–94.

[16] M.B. Haha, B. Lothenbach, G. Le Saout, F. Winnefeld, Influence of slag chemistry on the hydration of alkali-activated blast-furnace slag - Part II: Effect of Al2O3, Cem Concr Res 42 (1) (2012) 74–83, https://doi.org/10.1016/j.cemconres.2011.08.005.

[17] B.S. Gebregziabiher, R. Thomas, S. Peethamparan, Very early-age reaction kinetics and microstructural development in alkali-activated slag, Cem Concr Compos 55 (2015) 91–102, https://doi.org/10.1016/j.cemconcomp.2014.09.001.

[18] F. Puertas, Cementos de escorias activadas alcalinamente: Situación actual y perspectivas de futuro, Mater Constr 45 (239) (1995) 53–64, https://doi.org/10.3989/mc.1995.v45.i23910.3989/mc.1995.v45.i239.553.

[19] S. Song, D. Sohn, H.M. Jennings, T.O. Mason, Hydration of alkali-activated ground granulated blast furnace slag, J Mater Sci 35 (2000) 249–257, https://doi.org/10.1023/A:1004742027117.

[20] J.I. Escalante-García, A.F. Fuentes, A. Gorokhovsky, P.E. Fraire-Luna, G. Mendoza-Suarez, Hydration products and reactivity of blast-furnace slag activated by various alkalis, J Am Ceram Soc 86 (2003) 2148–2153, https://doi.org/10.1111/j.1151-2916.2003.tb03623.x.

[21] M. Ben Haha, G. Le Saout, F. Winnefeld, B. Lothenbach, Influence of activator type on hydration kinetics, hydrate assemblage and microstructural development of alkali activated blast-furnace slags, Cem Concr Res 41 (3) (2011) 301–310, https://doi.org/10.1016/j.cemconres.2010.11.016.

[22] M.B. Haha, B. Lothenbach, G. Le Saout, F. Winnefeld, Influence of slag chemistry on the hydration of alkali-activated blast-furnace slag — Part I: Effect of MgO, Cem Concr Res 41 (9) (2011) 955–963, https://doi.org/10.1016/j.cemconres.2011.05.002.

[23] S.A. Bernal, R. San Nicolas, R.J. Myers, R. Mejía de Gutiérrez, F. Puertas, J.S.J. van Deventer, J.L. Provis, MgO content of slag controls phase evolution and structural changes induced by accelerated carbonation in alkali-activated binders, Cem Concr Res 57 (2014) 33–43, https://doi.org/10.1016/j.cemconres.2013.12.003.

[24] C. Shi, Strength, pore structure and permeability of alkali-activated slag mortars, Cem Concr Res 26 (12) (1996) 1789–1799, https://doi.org/10.1016/S0008-8846(96)00174-3.

[25] F. Puertas, A. Fernández-Jiménez, M.T. Blanco-Varela, Pore solution in alkali-activated slag cement pastes. Relation to the composition and structure of calcium silicate hydrate, Cem Concr Res 34 (1) (2004) 139–148, https://doi.org/10.1016/S0008-8846(03)00254-0.

[26] R.J. Myers, S.A. Bernal, J.L. Provis, Phase diagrams for alkali-activated slag binders, Cem Concr Res 95 (2017) 30–38, https://doi.org/10.1016/j.cemconres.2017.02.006.

[27] O. Kayali, M.S.H. Khan, M. Sharfuddin Ahmed, The role of hydrotalcite in chloride binding and corrosion protection in concretes with ground granulated blast furnace slag, Cem Concr Compos 34 (8) (2012) 936–945, https://doi.org/10.1016/j.cemconcomp.2012.04.009.

[28] M.S.H. Khan, O. Kayali, U. Troitzsch, Effect of NaOH activation on sulphate resistance of GGBFS and binary blend pastes, Cem Concr Compos 81 (2017) 49–58, https://doi.org/10.1016/j.cemconcomp.2017.04.007.

[29] J. Péra, J. Ambroise, M. Chabannet, Properties of blast-furnace slags containing high amounts of manganese, Cem Concr Res 29 (2) (1999) 171–177, https://doi.org/10.1016/S0008-8846(98)00096-9.

[30] F. Puertas, Escorias de alto horno : composición y comportamiento hidráulico, Mater Construcción 43 (1993) 37–48, https://doi.org/10.3989/mc.1993.v43.i229.687.

[31] S.-D. Wang, K.L. Scrivener, P.L. Pratt, Factors affecting the strength of alkali-activated slag, Cem Concr Res 24 (6) (1994) 1033–1043, https://doi.org/10.1016/0008-8846(94)90026-4.

[32] A.G. De La Torre, S. Bruque, M.A.G. Aranda, Rietveld quantitative amorphous content analysis, J Appl Crystallogr 34 (2) (2001) 196–202, https://doi.org/10.1107/S0021889801002485.

[33] UNE 80225:2012. Methods of testing cement. Chemical analysis. Determination of reactive SiO2 content in cements, puzzolanas and fly ash 2012.

[34] UNE 196-2:2014. Method of testing cement. Part 2: Chemical analysis of cement. 2014.
[35] F. Pacheco-Torgal, J. Castro-Gomes, S. Jalali, Alkali-activated binders: A review. Part 2. About materials and binders manufacture, Constr Build Mater 22 (7) (2008) 1315–1322, https://doi.org/10.1016/j.conbuildmat.2007.03.019.
[36] UNE EN 196-6:2010. Methods of testing cement. Part 6: Determination of fineness 2010.
[37] UNE-EN ISO 17892-3:2018 Geotechnical investigation and testing - Laboratory testing of soil - Part 3: Determination of particle density 2018.
[38] UNE-EN 196-3:2017. Methods of testing cement - Part 3: Determination of setting times and soundness 2017.
[39] S.-D. Wang, X.-C. Pu, K.L. Scrivener, P.L. Pratt, Alkali-activated slag cement and concrete: a review of properties and problems, Adv Cem Res 7 (27) (1995) 93–102.
[40] F. Jin, K. Gu, A. Al-Tabbaa, Strength and hydration properties of reactive MgO-activated ground granulated blastfurnace slag paste, Cem Concr Compos 57 (2015) 8–16, https://doi.org/10.1016/j.cemconcomp.2014.10.007.
[41] Z. Shi, C. Shi, S. Wan, N. Li, Z. Zhang, Effect of alkali dosage and silicate modulus on carbonation of alkali-activated slag mortars, Cem Concr Res 113 (2018) 55–64, https://doi.org/10.1016/j.cemconres.2018.07.005.
[42] G. Renaudin, J. Russias, F. Leroux, F. Frizon, C. Cau-dit-Coumes, Structural characterization of C-S–H and C–A–S–H samples—Part I: Long-range order investigated by Rietveld analyses, J Solid State Chem 182 (12) (2009) 3312–3319, https://doi.org/10.1016/j.jssc.2009.09.026.
[43] S.K. Nath, S. Kumar, Reaction kinetics, microstructure and strength behavior of alkali activated silico-manganese (SiMn) slag – Fly ash blends, Constr Build Mater 147 (2017) 371–379, https://doi.org/10.1016/j.conbuildmat.2017.04.174.
[44] P. Parashar, V. Sharma, D.D. Agarwal, N. Richhariya, Rapid synthesis of hydrotalcite with high antacid activity, Mater Lett 74 (2012) 93–95, https://doi.org/10.1016/j.matlet.2011.12.115.
[45] H. Ye, C. Fu, G. Yang, Influence of dolomite on the properties and microstructure of alkali-activated slag with and without pulverized fly ash, Cem Concr Compos 103 (2019) 224–232, https://doi.org/10.1016/j.cemconcomp.2019.05.011.
[46] ASTM E178-08. Standard Practice for Dealing With Outlying Observations. 2008.
[47] J.M. Richardson, J.J. Biernacki, P.E. Stutzman, D.P. Bentz, Stoichiometry of Slag Hydration with Calcium Hydroxide, J Am Ceram Soc 85 (2002) 947–953, https://doi.org/10.1111/j.1151-2916.2002.tb00197.x.